Microporous and Mesoporous Materials 254 (2017) 146–152

Contents lists available at ScienceDirect

Microporous and Mesoporous Materials

journal homepage: www.elsevier.com/locate/micromeso

Novel preparation of CMK-3 nanostructured material modified with titania applied in hydrogen uptake and storage

Juliana M. Juárez, Brenda C. Ledesma, Marcos Gómez Costa, Andrea R. Beltramone*, Oscar A. Anunziata

Centro de Investigación en Nanociencia y Nanotecnología (NANOTEC), Facultad Regional Córdoba, Universidad Tecnológica Nacional, Maestro López y Cruz Roja Argentina, 5016, Córdoba, Argentina

ARTICLE INFO

Article history:
Received 28 September 2016
Received in revised form
24 February 2017
Accepted 28 March 2017
Available online 29 March 2017

Keywords:
Hard template method
Ti-SBA-15
Ti-CMK-3
Porous materials
Energy storage

ABSTRACT

This work deals with the development of a novel procedure to synthesize titania-modified nanostructured carbon employing Ti-SBA-15 as hard template. The new mesoporous carbon displays high specific surface area of 1044 m^2/g and large pore volume of 0.7 cm^3/g. XRD pattern of Ti-CMK-3 indicates that the ordered structure of this material is similar to the CMK-3. XRD, XPS and UV–Vis-DRS analysis indicated that Ti is highly dispersed as anatase phase in Ti-CMK-3. The synthesized Ti-CMK-3 exhibited significantly enhanced H_2 storage properties (2.6 wt%, equivalent to 13 mmol/g) compared with CMK-3 without Ti (2.2 wt%, 11 mmol/g) at 77 K and 10 bar.

1. Introduction

Ordered porous materials have attracted greater technological interest due to their high specific surface area, large pore volume and pore diameter, with applications including adsorption, catalysis, energy storage, gas separation and fuel cells [1–6]. Among the porous materials, mesoporous carbon materials with three-dimensional porous networks are highly interesting and believed to be more advantageous than porous materials having cubic pore structure with an ordered array of pores. Mesoporous carbon materials are very interesting from a scientific and technological viewpoint, due to their distinctive properties, such as chemical and thermal stability, adsorption capacity of different atoms, ions and supramolecules. The ordered mesoporous carbon (OMC) has a huge variety of applications such as catalysis, adsorption, energy and gas storage, separation and purification [7].

The synthesis of mesoporous carbons is usually carried out by nanocasting strategy, where the mesoporous silica material, called hard template, is impregnated with a suitable carbon precursor such as sucrose. After carbonization of the composite material, carbon replica is obtained by extracting the silica template. For instance, using ordered mesoporous silicas such as MCM-48 and SBA-15 as template, CMK-1 and CMK-3 are obtained. The pore size and pore distribution of the carbon replica depend on the wall thickness of the mesoporous silica template [8]. The resulting carbons are inverse replicas of ordered mesoporous silicas.

On the other hand, the incorporation of transition-metal ions into the frameworks of the molecular sieves is a general method for introducing catalytic sites into mesoporous material. For catalytic reactions according to Gutierrez et al. [9], the modification of mesoporous supports with Ti and Zr species significantly improves the performance of NiMo catalyst in HDS reactions. In our previous work [10], we observed that the presence of Ti-species on the surface of SBA-16 increased the strength of Ir interaction with the SBA-16-type support, leading to a distribution of Ir species more homogeneous than that on other pure silica supports. In the case of SBA-15, our previous works showed that the incorporation of titania molecules reduces significantly the size of iridium crystallites and improves its dispersion [11].

Hydrogen is an environmentally friendly fuel and a substitute energy source for many uses. Some advantages of using hydrogen as fuel includes simple adsorption-desorption kinetics, lightweight and low cost.

* Corresponding author.
E-mail address: abeltramone@frc.utn.edu.ar (A.R. Beltramone).

http://dx.doi.org/10.1016/j.micromeso.2017.03.056
1387-1811/

One of the most promising candidates in the gas separation and storage application are the Metal Organic Frameworks (MOF). Saha et al. [12] synthesized mixed crystals of MOF-5 and MOF-177 in order to determine hydrogen adsorption at a hydrogen pressure up to 1.05 bar and at different temperatures (77 K, 194.5 K and 298 K). Klyamkin et al. [13] studied the hydrogen storage properties up to 1000 bars of porous chromium (III) oxoterephthalate MIL-101 and hybrid MIL-101/Pt/C composite materials. These materials present 1.5 wt% of hydrogen sorption capacity compared with a maximum 0.4 wt% for pristine MIL-101.

Among the candidates of hydrogen physisorption, nanostructured carbons are one of the most interesting materials, due to their lightweight, low cost and abundant natural precursors. Carbons mesostructured from Korea (CMK) belong to such family of ordered mesoporous carbons (OMC) [14].

This type of material is synthesized inside the channels of mesostructured silicates, and is characterized for their high specific surface areas, from 1000 to 2000 m^2/g, and pore volumes from 0.5 to over 1 mL/g. Such characteristics make them so interesting for hydrogen storage applications.

Metal particles dispersed in the porosity of active carbons contribute to improve the storage capacity. The H_2 adsorption of CMK-1 was around 1.2 wt% at 1 bar and the activated CMK-3 around 2%. Juárez et al. [15,16], reported Pt-CMK-3, Zn-CMK-1 and Ni-CMK-3 as promising hydrogen storage nanomaterials. The adsorption in these materials was fully reversible and higher than that in carbon hosts.

TiO_2 is one of the important metal oxides for a broad range of H_2 gas sensing applications because of its surface chemistry and structure, charge transport and electrical properties. Anatase, rutile and brookite are natural polymorphs of TiO_2. The brookite phase has mechanical and thermal properties similar to those of the rutile phase. The rutile phase is a thermodynamically more stable phase than the anatase phase at high temperature. However, it has been shown that electron transport is slower in the rutile and brookite layers than in the anatase layer because of a difference in the extent of inter-particle connectivity associated to particle packing density [17].

Han et al. [18] studied the influence of different Ti doping levels in the SBA-15 materials for the hydrogen capacity; and found that the Ti substitution and/or dispersion in the silica framework was activated and the hydrogen adsorption capacity was enhanced.

In this work, we present an easy, novel and productive method for successfully obtaining an ordered mesoporous carbon modified with titania, using Ti containing-siliceous hard template, with good results such as high dispersion and lower nanoclusters of titania on the inner nanostructured carbon walls and higher H_2 storage.

The originality of this work is the novel material obtained. The new synthesis by nanocasting method using Ti-SBA-15 as template was not reported in literature and it presents a promising technique to develop mesoporous carbons with highly dispersed nanoparticles of titania in the anatase phase. The new nanomaterial it is also a great candidate for hydrogen uptake, improving the storage of the typical CMK-3 without TiO_2 nanoparticles.

2. Materials and methods

2.1. Synthesis of SBA-15

Ordered mesoporous silica SBA-15 was prepared according to the procedure described by Zhao et al. [19]. By using triblock copolymer, poly(ethylene glycol)-block-poly-(propylene glycol)-block-poly (ethylene glycol) as the surfactant and tetraethylorthosilicate as silica source, 9.1 g of P123 were dissolved in 288 mL of HCl (2 M). The temperature of P123 solution was controlled at 50 °C. After that, 22.2 mL of TEOS were added to P123 solution under stirring for 20 min; the resultant solution was maintained in static condition for 24 h. The resultant mix was transferred to a Teflon bottle and maintained at 80 °C for 24 h without stirring. The sample was calcined at 550 °C for 5 h to remove the copolymer template.

2.2. Synthesis of Ti-SBA-15

Ti-SBA-15 was synthesized using Tetraethylorthosilicate (TEOS, 98%, Sigma–Aldrich), Tetraethylorthotitanate (TEOT, 98% Sigma–Aldrich), Pluronic 123 in acidic medium. 9 g of P123 were dissolved in 288 mL of HCl (2 M). The temperature of P123 solution was controlled at 50 °C. After that, 21.2 mL of TEOS were added to P123 solution under stirring for 20 min; 1.4 mL of TEOT were then added to the resultant solution and maintained in static condition for 24 h. The resultant mix was transferred to a Teflon bottle and maintained at 80 °C for 24 h without stirring. The sample was calcined at 550 °C for 5 h to remove the copolymer template. This sample was synthesized with a Si/Ti = 20 ratio.

2.3. Synthesis of mesoporous carbon CMK-3 and Ti-CMK-3

The mesoporous carbon Ti-CMK-3 was synthesized using the nanocasting strategy, via a two-step impregnation of the mesopores of Ti-SBA-15 (Si/Ti = 20) with a solution of sucrose as source of carbon using an incipient wetness method. In order to obtain CMK-3, the hard template used in the synthesis was SBA-15 prepared according to previous work [15]. Briefly, 1 g of the mesoporous template (SBA-15/Ti-SBA-15) was impregnated with an aqueous solution of $H_2SO_4$with 1.1 g of the carbon precursor (0.14 g of H_2SO_4 in 5 g of deionize water with 1.1 g of sucrose). Afterwards, both mixtures were dried at 110 °C for 6 h and at 160 °C for another 6 h. Both samples were treated again at 100 and 160 °C after the addition of 0.65 g of sucrose, 90 mg of H_2SO_4 and 5.0 g of deionized water. The sucrose-SBA-15 and sucrose-Ti-SBA-15 samples were then carbonized under nitrogen atmosphere at 900 °C. The silica in both samples was removed using a solution of hydrofluoric acid 5 wt% at room temperature. After two dissolutions of the silica, the samples were filtered, washed with deionized water and ethanol, and dried at 50 °C, overnight. The samples were denoted as CMK-3 and Ti-CMK-3.

2.4. Characterization

X-ray diffraction analyses were obtained with a PANANALITYCAL Phillips X'pert XDS diffractometer with a diffractometer beam monochromator and CuKα radiation source. N_2 adsorption/desorption isotherms at 77 K were measured on ASAP 2020 equipment, after degassing the samples at 400 °C, determining textural properties such as surface area and pore volume. The pore size distribution of Ti-SBA-15 was determined by the Nonlocal Density Functional Theory (NLDFT) dedicated for cylindrical pores of siliceous adsorbents at 77 K, using the adsorption branch; whereas the quenched solid density functional theory (QSDFT) was used to determine the pore size distribution of CMK-3 and Ti-CMK-3 at 77 K on carbon (slit-cylindrical pores, adsorption branch). The same models were applied to calculate micro- and mesopore volumes. Scanning electron microscopy (SEM) micrographs were obtained by using a Nova NANOSEM 230 with energy dispersive X-ray spectroscopy (EDS) (FEI Company, Oregon, USA). Ultraviolet–visible diffuse reflectance spectroscopy (UV–Vis-DRS) was used to determined the Ti species in the samples, recorded with a PerkinElmerLamba 650 spectrophotometer equipped with a diffuse reflectance accessory. X-ray Photoelectron Spectra (XPS)

were obtained on a MicrotechMultilb 3000 spectrometer, equipped with a hemispherical electron analyzer and MgKα (hν = 1253.6 eV) photon source. An estimated error of ±0.1 eV can be assumed for all measurements. Raman spectrum was obtained from an InVia Reflex Raman microscope and spectrometer using a 532 nm diode laser excitation. TEM micrographs were obtained on a JEOL model JEM-1200 EX II microscope. H_2 storage isotherms at 77 K at low and high pressure (up to 10 bars) were measured using ASAP 2050 equipment correctly calibrated.

3. Results and discussion

3.1. XRD

Fig. 1(a) shows the XRD patterns of the hard templates (SBA-15 and Ti-SBA-15) and of CMK-3 and Ti-CMK-3. Patterns of SBA-15 and Ti-SBA-15 present three peaks around 2θ = 0.80, 1.4 and 1.6, characteristic of this kind of mesoporous material indexed to the planes [100], [110] and [200]. There is a slight shift in the [100] peak to higher 2θ values and a lower spacing in the samples with Ti. The shift in higher unit cell parameter (a_0) may be attributed to longer Ti–O bond length compared to that of Si–O bond. Such an observation indicates successful incorporation of Ti into SBA-15 structure.

The pattern of CMK-3 has three diffraction peaks, indexed as [100], [110] and [200] planes associated with hexagonal symmetry, identical to SBA-15 structure, indicating that the ordered structure is an exactly negative replica of mesoporous silica SBA-15. In the case of the novel Ti-CMK-3, the pattern shows the same peaks as those of CMK-3, suggesting that the ordered structure of this material is similar to that of CMK-3 without Ti. However, it shows a slight shift to higher angles with a decrease in the unit cell parameter (a_o). A shift to higher values may mean that the material has a better structural order. Two other factors that contribute to peak shift and wider signal comprise residual stress and defects in the material, since they can also deform the lattice.

Fig. 1 (b) shows the wide-angle XRD pattern of the samples synthesized. In both samples two broad diffraction peaks are distinguished and can be indexed as [0 0 2] and [1 0 0] diffraction for typical graphite carbons [20]. In the wide-angle region, practically no reflections typical of titanium have been found in the Ti-CMK-3 sample. It only can be indexed a characteristic peak assigned to the plane [101] of anatase phase. The absence of these prominent reflections and of the cubic titanium carbide phase reflections at 2θ = 36.208, 42.008, 60.708, 72.608, and 76.708, indexed to the [111], [200], [220], [311], and [222] respectively, according to the standard powder diffraction file (PDF) 38-1420, indicates that no crystalline bulk material has been formed outside the pore system. It is an evidence that clusters have nanometric size and high dispersion [21], demonstrating that the nanoparticles could be inside the channels of CMK-3.

3.2. Analysis of adsorption/desorption isotherms

N_2 adsorption–desorption isotherms and pore size distribution for both mesoporous carbons are shown in Fig. 2(a) and (b). Both curves are type IV, characteristic of mesoporous materials with a marked leap in the adsorption at a relative pressure P/P_0 of 0.4–0.6. In addition, the two samples show high specific surface area, higher than 1000 m^2/g, high pore volume and narrow mesopore size distribution (Table 1). The BET surface area for the sample without Ti is 1323 m^2/g, the pore volume is 1.1 m^3/g, and the average pore diameter is 5.2 nm. On the other hand, the BET surface area of the Ti-CMK-3 is 1044 m^2/g, the pore volume is 0.78 m^3/g, and the pore diameter is 4.1 nm. There is a decrease in all textural properties of the novel nanomaterial due to the incorporation of the nanoclusters of titania into the mesoporous carbon CMK. Based on XRD, TEM and pore size distribution results, we can conclude that the ordered mesoporous structure has been retained, and no collapse of carbon framework occurs with the incorporation of Ti in the structure of CMK-3.

3.3. UV–Vis of Ti-SBA-15 and Ti-CMK-3

UV–Vis diffuse reflectance spectroscopy (UV–Vis–DRS) (Fig. 3) was used to study the dispersion and chemical environment of Ti incorporated in SBA-15 and CMK-3 matrix. The spectra of Ti-SBA-15 shows a band at 210 nm, corresponding to tetragonal titanium with $Ti(OSi)_4$ structure [22], absent in Ti-CMK-3 sample. The result indicates that, the Ti species introduced are well dispersed in the SBA-15mesoporous employed as hard template. Ti-CMK-3 presents a band at 240-320 corresponding to octahedral isolated Ti species corroborating the anatase phase [22]. The absence of the absorption band at higher wavelength range indicates that the size of the

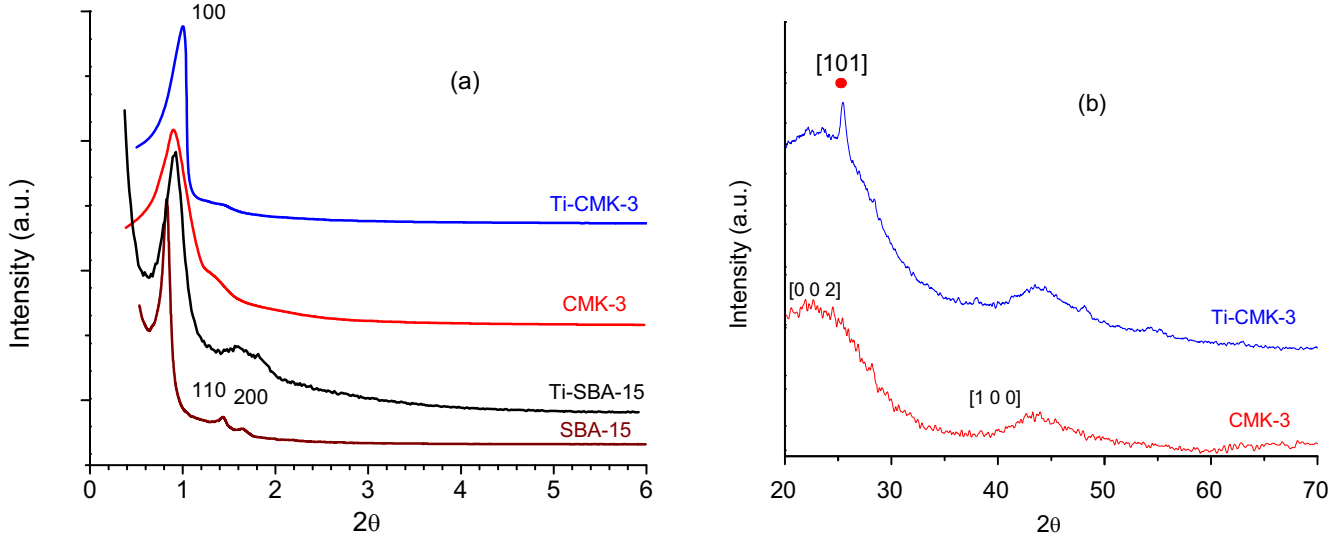

Fig. 1. a) Low angle XRD patterns, b) wide-angle XRD.

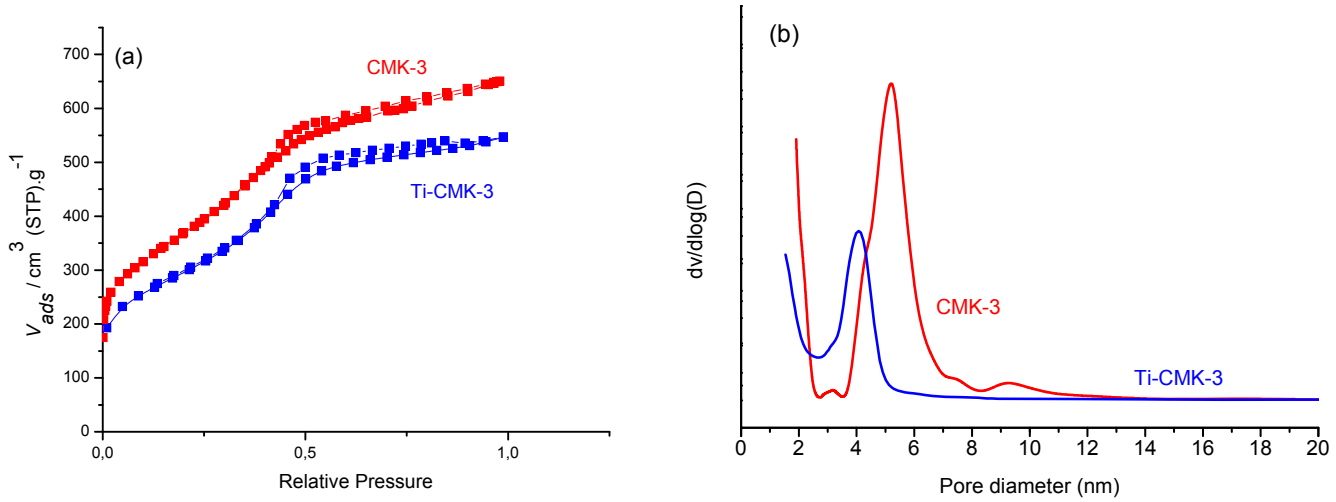

Fig. 2. a) N_2 adsorption–desorption isotherms, b) pore size distribution of the samples synthesized.

Table 1
Textural properties.

Material	S_{BET} (m^2 g^{-1})[a]	V_{TP} (cm^3 g^{-1})[b]	$V_{\mu P}$ (cm^3 g^{-1})[b]	W_p (nm)[b]	H_2 uptake (wt.%)[c]
Ti-CMK-3	1044	0.78	0.17	4.1	2.6
CMK-3	1323	1.10	0.25	5.2	2.2
Ti-SBA-15	1020	1.30	0.09	7.0	–

[a] Determined by BET specific surface area (±2%).
[b] Calculated by NLDFT/QSDFT method from the adsorption branch.
[c] H_2 sorption at 10 bars and 77 K.

pore channels of CMK-3 avoids the growing of the TiO_2 particles, obtaining a very small size of the nanocrystal of anatase.

3.4. Raman studies

Fig. 4 shows the Raman spectra of the samples Ti-CMK-3 and pure rutile and anatase as references. The spectra are in the range of 300–900 cm-^{1} in order to corroborate the nature of de titania nanoparticles. We can observe in Ti-CMK-3 spectrum the characteristic signals of anatase [23], and no signal corresponding to rutile. We can conclude that all titanium has been incorporated as anatase phase.

3.5. TEM, SEM and EDX studies

TEM image of the samples are illustrated in Fig. 5 (a). Domains of ordered hexagonal arrays, which exhibited a uniform array of

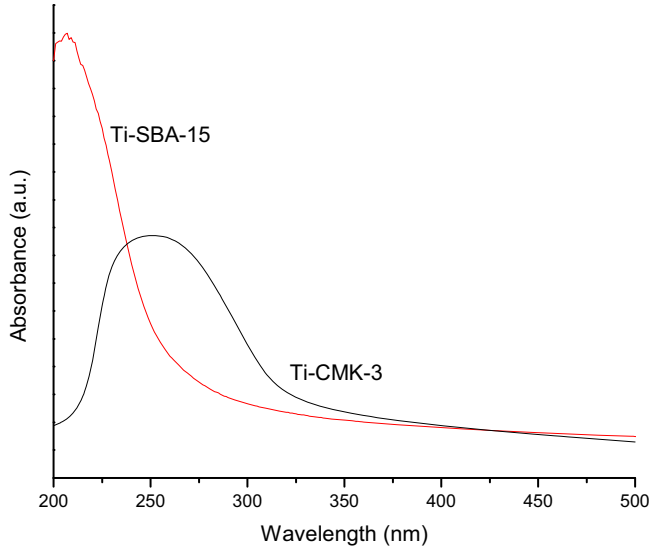

Fig. 3. UV–Vis–DRS of Ti-SBA-15 and Ti CMK-3 samples.

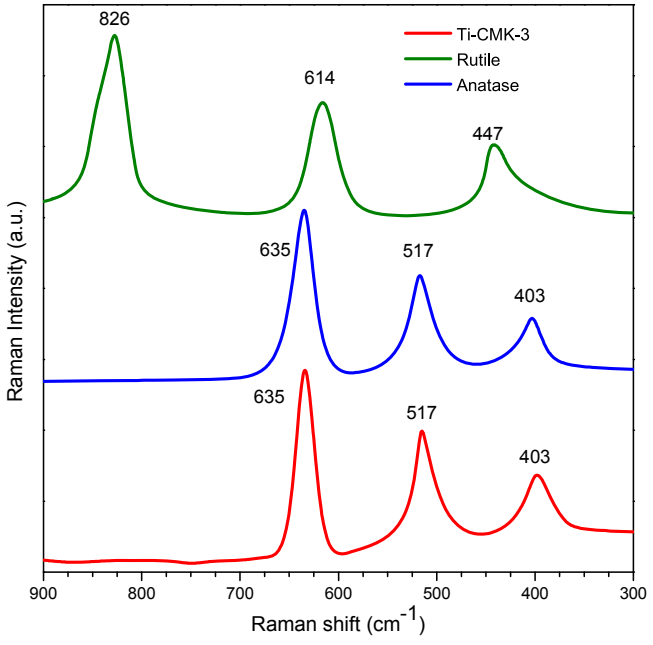

Fig. 4. Raman spectra of Ti-CMK-3, rutile and anatase.

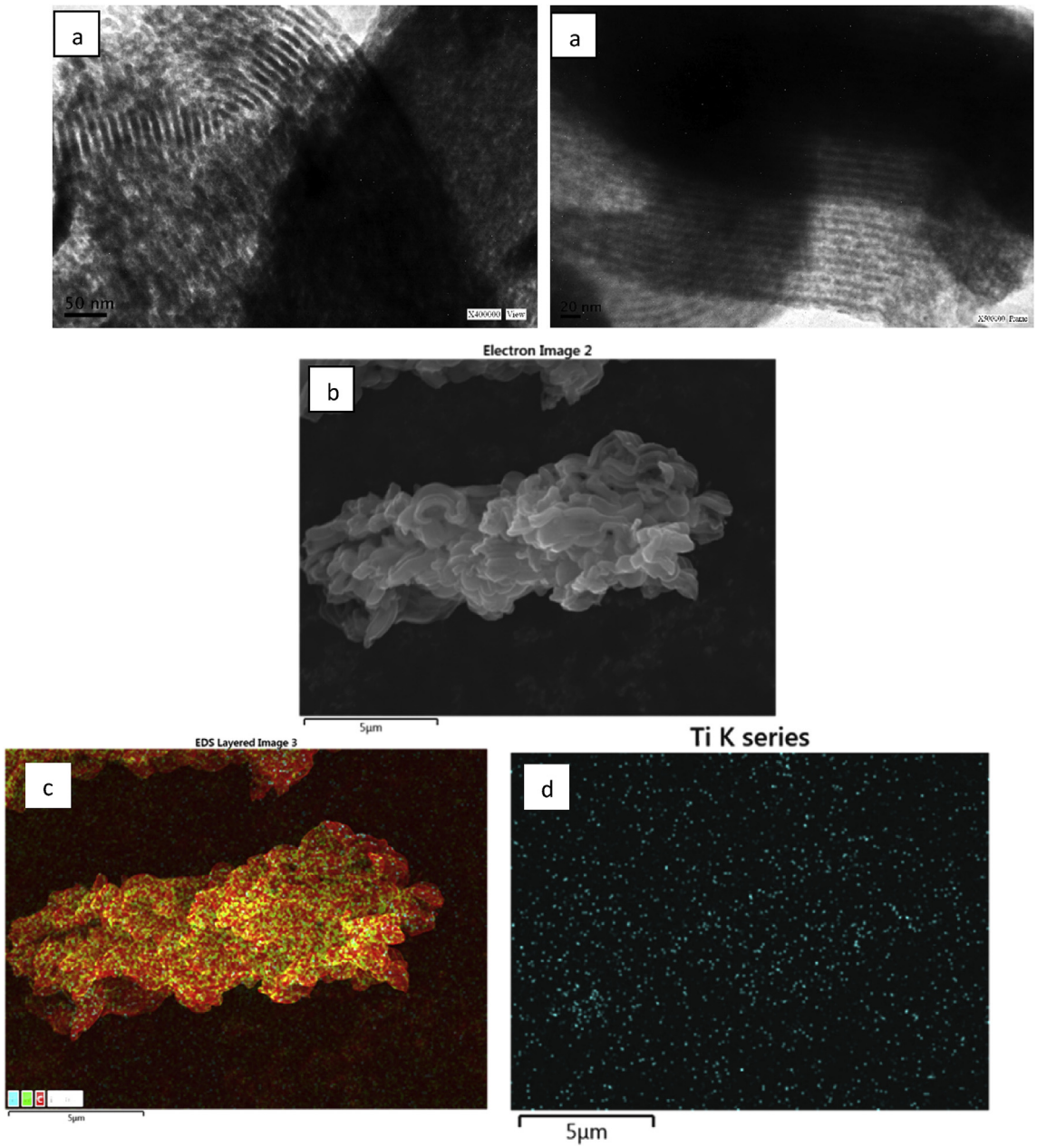

Fig. 5. (a) TEM images, (b) SEM image, (c) corresponding EDX elemental mappings of C, Ti and O, (d) Ti K series of Ti-CMK-3.

mesopores with a long-range order, are observed in Ti-CMK-3 sample. The image proves that the pore structure of the pristine Ti-SBA-15 is preserved on the carbon material. SEM image shown in Fig. 5(b) is characteristic of CMK-3 crystallites.

In order to verify the composition of Ti-CMK-3 sample, energy-dispersive X-ray spectroscopic (EDX) characterization and elemental mapping of our material were carried out (Fig. 5 (c) and 5(d)). The results show evidence about C, Ti and O distribution onto the Ti-CMK-3 matrix. They further confirm the embedding characteristics of mesoporous CMK-3 [24]. The panoramic view shown in Fig. 5 indicates that the sample was not affected by the incorporation of Ti. From EDX measure and elemental mapping, uniform distribution of Ti atoms was also confirmed. By Map Sum Spectrum, the elemental composition of Ti-CMK-3 indicate that Ti is implanted in C framework of CMK-3 as anatase phase, Ti/C = 0.003 (around 1.05 wt%) with the absence of silica from the hard template. Whereas by XPS analysis of Ti-CMK-3 (not shown), indicate that Ti is incorporated in the mesoporous nanostructure of CMK-3 as anatase phase [25,26] (Ti 2p3/2 signal at 458.5 eV), with Ti/C = 0.00042 showing that Ti species are well dispersed in the mesopores of CMK-3. The lower value found by XPS indicates that Ti is mostly in the inner surface of the material.

3.6. Hydrogen uptake measurement

The ability of hydrogen storage was measured at different pressures and cryogenic temperatures (77 K). Freundlich isotherm equation was used to fit experimental data. The Freundlich model has been described in our previous work [15]. Fitting accuracy was R^2 = 0.98. Fig. 6 shows the adsorption–desorption Freundlich isotherms of hydrogen at 77 K on CMK-3 and Ti-CMK-3 samples at a range of pressure (0–10 bar). As we can see in this Figure, Ti-CMK-3

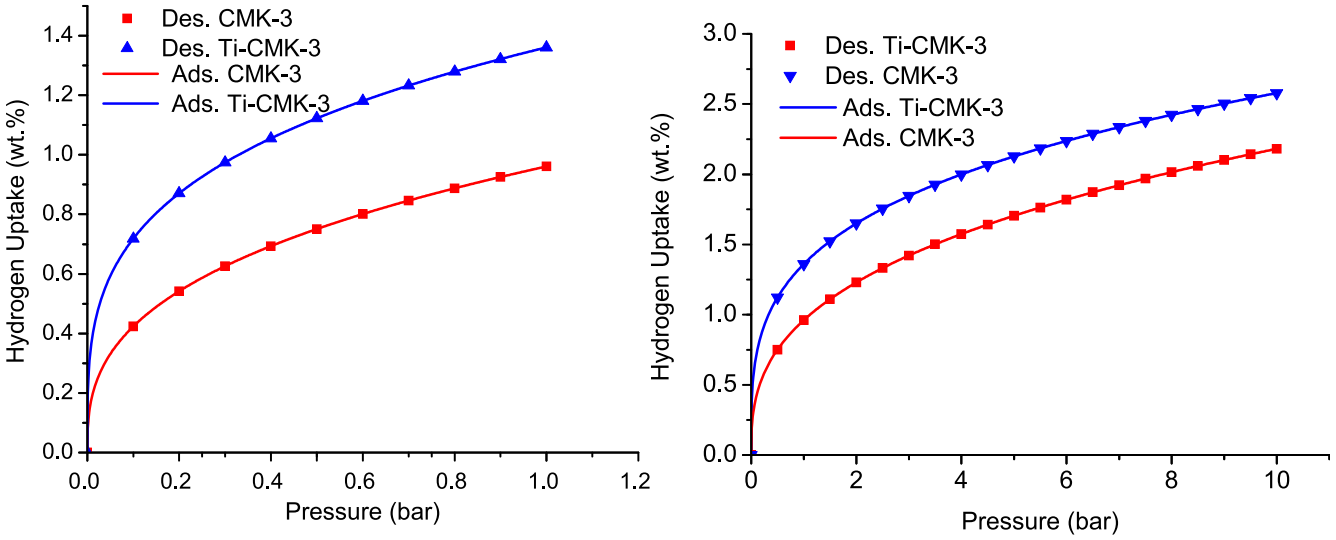

Fig. 6. H_2 adsorption–desorption isotherms of CMK-3 and Ti-CMK-3.

and CMK-3 carbons are not comparable in terms of hydrogen storage. Ti-CMK-3 has anatase nanoclusters dispersed in CMK-3 framework, which increases hydrogen storage in CMK-3 carbon. As seen in the Figure the process of hydrogen uptake was completely reversible [27], indicating absence of strong bond between hydrogen and anatase nanocluster or CMK-3 framework [15].

CMK-3 surface promotes high surface areas of anatase nanoclusters, which is important to cause hydrogen adsorption (H_2 molecules) by weak chemical pathways (such as dihydrogen complex interaction). Through XRD and EDX characterization, we also noticed that, with the assistance of CMK-3, anatase nanoparticles show small size and high dispersion, contributing to the substantial increase in H_2 adsorption. In other words, the presence of anatase nanoclusters in CMK-3 results in formation of better-localized states of electrons in the anatase nanoclusters.

Since the amount of Ti could affect the hydrogen uptake, we choose a Si/Ti = 20 as the optimal ratio, in order to obtain the better dispersion and small size of the anatase nanoparticles. In a previous [28] work we studied the incorporation of different content of titanium in SBA-16 mesoporous material and we observe that the better dispersion was obtained with Si/Ti = 20, when higher Si/Ti ratios (between 15 and 10) were intend the anatase clusters were larger or the structure collapsed. The best titanium dispersion was obtained with Si/Ti ratio of 20.

There are two different processes involved in the hydrogen adsorption on the Ti-CMK-3 surface: hydrogen molecules can spill over onto CMK-3 nano/micropores and adsorbed onto nanometric anatase clusters.

Anatase nanoclusters containing in CMK-3 results in formation of better localized states of electrons at anatase nanoclusters than rutile. These localized states may distribute electron concentration at the surface of Ti-CMK-3 composite and causes weak bonds between hydrogen molecules and surface TiO_2 nanoclusters [29].

Anatase has a band gap greater than rutile. As the energy band gap is different, the Ti-Ti distances in anatase clusters are larger than in rutile. This change affects the mass density and results in a different electronic configuration. Rutile phase presents more pronounced localization of 3d states and therefore a narrower 3d bands. This increases the “power” of the electron oxidation and facilitates the transfer of electrons from the TiO_2 to the adsorbed molecules. This explanation has also been extended to explain the activities that depend on surface orientation by suggesting that different areas have different band intervals [30]. Moreover, anatase displays an indirect band gap and this is smaller than its direct band gap. Semiconductors that have indirect band gap generally exhibit life times longer of charge carriers compared to direct gap materials. A longer life of electron-hole pair in anatase than in rutile would make it more probably to involve in surface reactions the charge carriers [30].

According to theoretical investigations of Shalabi et al. [31], the adsorption of the first H_2 molecule is therefore dissociative, with Ti–H bond. The adsorption of the first H_2 molecule does not affect the distance between Ti and the nearest C and consequently does not affect the strength interaction between TiO_2 and CMK-3. The mixed sp^2d hybridization of Ti–C bonds seems to have strong repulsive effects on the adsorbed H_2 leading to elongation of H–H distance. Hydrogen atoms of the adsorbed H_2 molecule should have negative charges, H_2 molecule can be considered as trapped by Ti cation via the charge polarization mechanism. This indicates that Ti donates electrons to neighboring C atoms on CMK-3, where the d-orbitals of Ti atom overlap with the sp^2 orbitals of Ti–C bonds to form the mixed sp^2d hybridization. This charge transfer behavior is possible since Ti atom is in cationic form and renders extensive hetero polar bonding between the Ti atom and the nearest C atoms, resulting in an increase in H_2 molecule uptake. Moreover, CMK-3 approaching the positively charged Ti cation leads to loss of d-orbital degeneracy as the electrons of CMK-3 will be closer to some of d- orbitals while farther away from others. Thus, d- orbitals closer to CMK-3 have a higher energy than those farther away. This results in d- orbitals splitting in energy to reduce total energy and stabilize the system as explained by ligand field theory [32].

The first layer of hydrogen molecules can interact through anatase clusters as dihydrogen complex [27,33]; however, the amount of hydrogen adsorbed is negligible. The second layer of hydrogen molecules is physically adsorbed through dipole-induced interactions. Hydrogen molecules are non-polar, but dipole-induced effects in hydrogen molecules are generated by anatase particles due to the strong interaction between clusters. The third layer and any upper layer of hydrogen molecules could interact with metal cluster by the same mechanism. This mechanism can be applied at higher pressure; consequently, Ti-CMK-3 adsorbs a higher amount of hydrogen than CMK-3 mesoporous carbon at higher pressures.

According to existing bibliography, the adsorption of hydrogen at room temperature has similar behavior that at 77 K, but with significantly lowers adsorption. Campesi et al. [34] measured hydrogen adsorption onto an organized mesoporous carbon with PdNi alloy nanoparticles and a Pd nanoparticle/carbon template composite [35] at 77 K and 298 K. In the first work, adsorption was about 0.85 wt % at 77 K and 0.045 wt % at 298 K (2 MPa). In the second, was approximately 1.0 wt % at 77 K (1.5 Mpa) and 0.08 wt % at 298 K (0.5 Mpa).

4. Conclusions

In this work, a novel mesoporous carbon modified with titania was prepared incorporating Ti species from the hard template Ti-SBA-15 material. The titania incorporated in the mesoporous carbon is in the anatase phase according to XRD, Raman and UV–Vis-DRS analyses. The new material has high specific surface area, pore volume and narrow mesopore size distribution. EDX mapping and quantification, with highly dispersed Ti species, suggest that TiO_2 is confined into the carbon framework of CMK-3. In addition, it is also found that the hydrogen storage capacity of this novel mesoporous carbon with titania is increased from 2.2 wt% (11 mmol/g) to 2.6 wt % (13 mmol/g) at 77 K and 10 bar.

Acknowledgements

Juliana M. Juárez, Brenda C. Ledesma, Andrea R. Beltramone, Marcos Gómez Costa, Oscar A. Anunziata, NANOTEC, CONICET, National Technology University, Cordoba Faculty, Maestro Lopez y Cruz Roja Argentine. We acknowledge the financial support of CONICET Argentina, PIP CONICET 11220120100218CO. 2014–2017.

References

[1] K. Ariga, A. Vinu, Y. Yamauchi, Q. Ji, J.P. Hill, Bull. Chem. Soc. Jpn. 85 (2012) 1–32.
[2] S.H. Joo, S.J. Choi, I. Oh, J. Kwak, Z. Liu, O. Terasaki, R. Ryoo, Nature 412 (2001) 169–172.
[3] X. Jin, V.V. Balasubramanian, S.T. Selvan, D.P. Sawant, M.A. Chari, G.Q. Lu, A. Vinu, Angew. Chem. Int. Ed. 48 (2009) 7884–7887.
[4] A. Vinu, P. Srinivasu, M. Takahashi, T. Mori, V.V. Balasubramanian, K. Ariga, Micropor. Mesopor. Mat. 100 (2007) 20–26.
[5] A. Vinu, M. Miyahara, K. Ariga, J. Phys. Chem. B 109 (2005) 6436–6441.
[6] W. Zhuang, Y. Wan, C. Feng, Y. Shen, D. Zhao, Chem. Mater. 21 (2009) 706–716.
[7] M. Enterria, F.S. Garcia, A.M. Alonso, J.M.D. Tascon, Micropor. Mesopor. Mater. 151 (2012) 390–396, 151.
[8] J. Lang, X. Yan, X. Yuan, J. Yang, Q. Xue, J. Power Sources 196 (2011) 10472–10478.
[9] O. Gutiérrez, G. Fuentes, C. Salcedo, T. Klimova, Catal. Today 116 (2006) 485–497.
[10] B.C. Ledesma, V.A. Valles, L.P. Rivoira, M.L. Martinez, O.A. Anunziata, A.R. Beltramone, Catal. Lett. 144 (2014) 783–795.
[11] B.C. Ledesma, O.A. Anunziata, A.R. Beltramone, Appl. Catal. B 192 (2016) 220–233.
[12] D. Saha, S. Deng, Int. J. Hydrogen Energy 34 (2009) 2670–2678.
[13] S. Klyamkin, S. Chuvikov, N. Maletskaya, E. Kogan, V. Fedin, K. Kovalenko, D. Dybtsev, Int. J. Hydrogen Energy 38 (2014) 1562–1570.
[14] H. Yang, D. Zhao, J. Mater. Chem. 15 (2005) 1217–1231.
[15] J.M. Juárez, M.B. Gómez Costa, O.A. Anunziata, Int. J. Energy Res. 39 (2015) 128–139.
[16] J.M. Juárez, M.B. Gómez Costa, O.A. Anunziata, Int. J. Energy Res. 39 (2015) 941–953.
[17] S. Nasirian, H. Milani Moghaddam, Int. J. Hydrogen Energy 39 (2014) 630–642.
[18] Y. Han, H. Kim, J. Park, J. Kim, Int. J. Hydrogen Energy 37(3012) 14240–14247.
[19] Y. Zhao, J. Feng, Q. Huo, N. Melosh, G.H. Fredrickso, B.F. Chmelka, G.D. Stucky, Science 279 (1998) 548–552.
[20] U. Suryavanshi, T. Iijima, A. Hayashia, Y. Hayashi, M. Tanemura, Chem. Eng. J. 179 (2012) 388–393.
[21] M.B. Gómez Costa, J.M. Juárez, M.L. Martínez, A.R. Beltramone, J. Cussa, O.A. Anunziata, Mater. Res. Bull. 48 (2013) 661–667.
[22] G. Petrini, A. Cesana, G.F. De Alberti, G. Genoni, M. Leofanti, M. Padovan, G. Paparatto, P. Roffia, Stud. Surf. Sci. Catal. 68 (1991) 761–766.
[23] S. Balaji, Y. Djaoued, J. Robichaud, J. Raman Spectrosc. 37 (2006) 1416–1422.
[24] W. Hsuan Hung, S.N. Lai, A.Y. Lo, Appl. Mater. Interfaces 7 (2015) 8412–8418.
[25] D.C.M. Dutoit, M. Schneider, R. Hutter, A. Baiker, J. Catal. 161 (1996) 651–658.
[26] V.V. Atuchin, V.G. Kesler, N.V. Pervukhina, Z. Zhang, J. Electron. Spectrosc. Relat. Phenom. 152 (2006) 18–24.
[27] B.-J. Kim, S.-J. Park, Int. J. Hydrogen Energy 36 (2015) 648–653.
[28] L. Rivoira, V. Vallés, B. Ledesma, M. Ponte, M. Martínez, O. Anunziata, A. Beltramone, Catal. Today 271 (2016) 102–113.
[29] T.K.A. Hoang, D.M. Antonelli, Adv. Mater 21 (2009) 1787–1800.
[30] T. Luttrell, S. Halpegamage, J. Tao, A. Kramer, E. Sutter, M. Batzill, Sci. Rep. 4 (2014) 40–43.
[31] A.S. Shalabi, H.O. Taha, K.A. Soliman, S. Abeld, J. Power Sources 271 (2014) 32–41.
[32] L.P. Zhang, P. Wu, M.B. Sullivan, J. Phys. Chem. C 115 (2011) 4289–4296.
[33] Y. Takasu, R. Unwin, B. Tesche, A.M. Bradshaw, M. Grunze, Surf. Sci. 77 (1978) 219–232.
[34] R. Campesi, F. Cuevas, E. Leroy, M. Hirscher, R. Gadiou, C. Vix-Guterl, M. Latroche, Micropor. Mesopor. Mat. 117 (2009) 511–514.
[35] R. Campesi, F. Cuevas, R. Gadiou, E. Leroy, M. Hirscher, C. Vix-Guterl, M. Latroche, Carbon 46 (2008) 206–214.